Immunity, Vol. 12, 51–60, January, 2000, Copyright ©2000 by Cell Press

Structure and Dimerization of a Soluble Form of B7-1

Shinji Ikemizu,* Robert J. C. Gilbert,*‡ Janet A. Fennelly,† Alison V. Collins,† Karl Harlos,*‡ E. Yvonne Jones,*‡ David I. Stuart,*‡§ and Simon J. Davis†§

*Division of Structural Biology
Wellcome Trust Centre for Human Genetics
The University of Oxford
Roosevelt Drive
Oxford OX3 7BN
United Kingdom

†Nuffield Department of Clinical Medicine
The University of Oxford
John Radcliffe Hospital
Headington, Oxford OX3 9DU
United Kingdom

‡Oxford Centre for Molecular Sciences
The University of Oxford
New Chemistry Laboratory
South Parks Road
Oxford OX1 3QT
United Kingdom

Summary

B7-1 (CD80) and B7-2 (CD86) are glycoproteins expressed on antigen-presenting cells. The binding of these molecules to the T cell homodimers CD28 and CTLA-4 (CD152) generates costimulatory and inhibitory signals in T cells, respectively. The crystal structure of the extracellular region of B7-1 (sB7-1), solved to 3 Å resolution, consists of a novel combination of two Ig-like domains, one characteristic of adhesion molecules and the other previously seen only in antigen receptors. In the crystal lattice, sB7-1 unexpectedly forms parallel, 2-fold rotationally symmetric homodimers. Analytical ultracentrifugation reveals that sB7-1 also dimerizes in solution. The structural data suggest a mechanism whereby the avidity-enhanced binding of B7-1 and CTLA-4 homodimers, along with the relatively high affinity of these interactions, favors the formation of very stable inhibitory signaling complexes.

Introduction

The course of an immune response is in large part controlled by the interactions of leukocyte cell surface molecules. Among the most important are those involving the B7 molecules B7-1(CD80) and B7-2(CD86), which are expressed on antigen-presenting cells and bind to both CD28 and CTLA-4(CD152) expressed on T cells (reviewed by Lenschow et al., 1996; Greenfield et al., 1998). Altering these interactions has profound effects on immune responses in experimental disease models. Enhanced anti-tumor immune responses result from transfecting B7-1 into murine tumors (Chen et al., 1992; Townsend and Allison, 1993) or from using anti-CTLA-4 antibodies to block CTLA-4 interactions with B7-1 and B7-2 (Leach et al., 1996). Conversely, inhibition of B7/CD28 interactions results in general immunosuppression (Linsley et al., 1992b), reduced autoantibody production (Finck et al., 1994), and enhanced skin and cardiac allograft survival (Larsen et al., 1996). There is, therefore, considerable interest in the therapeutic potential of manipulating human B7 interactions, and such approaches have already shown promise (Guinan et al., 1999).

B7-1 and B7-2 each consist of single V-like and C-like immunoglobulin superfamily (IgSF) domains (Freeman et al., 1989, 1993a; Azuma et al., 1993). Their ligands, CD28 and CTLA-4, are also structurally related and are expressed at the cell surface as homodimers of single V-like IgSF domains (Aruffo and Seed, 1987; Brunet et al., 1987). A third CD28-like molecule, ICOS (Hutloff et al., 1999), interacts with another B7-related molecule (D. Brodie et al., unpublished data), but the analysis of transgenic mice indicates that B7-1 and B7-2 are the only functional ligands of CD28 and CTLA-4 (Mandelbrot et al., 1999). The affinities of these interactions differ substantially: human CTLA-4 binds B7-1 with a solution K_d of 0.2–0.4 μM (van der Merwe et al., 1997), whereas the affinity of CD28 for B7-2 is 40- to 100-fold lower (B7-1/CD28 and B7-2/CTLA-4 interactions each have intermediate affinities [$K_d = 4$ μM]; A. V. C. et al., unpublished data).

The expression of B7-1, B7-2, CD28, and CTLA-4 is tightly regulated: whereas CD28 is constitutively expressed on resting human T cells and B7-2 is rapidly induced on antigen-presenting cells early in immune responses, the expression of both B7-1 and CTLA-4 is considerably delayed (reviewed by Lenschow et al., 1996). Interactions of the B7 molecules with CD28 generate costimulatory signals amplifying T cell receptor (TCR) signaling and preventing anergy, whereas interactions with CTLA-4 induce powerful inhibitory signals in T cells (Martin et al., 1986; Weiss et al., 1986; Harding et al., 1992; Walunas et al., 1994; Waterhouse et al., 1995). CD28-dependent costimulation is poorly understood, but recent work implicates the bulk recruitment of cell surface molecules and kinase-rich rafts to the site of TCR engagement, favoring receptor phosphorylation and signaling (Viola et al., 1999; Wülfing and Davis, 1999). Conversely, CTLA-4 inhibits signal transduction by recruiting the tyrosine phosphatase SHP-2 to the TCR, resulting in dephosphorylation of the ζ chain of the complex and components of the RAS signaling pathway (Marengere et al., 1996; Lee et al., 1999), and by interfering with distal events in the CD28 signaling pathway (Olsson et al., 1999).

While the opposing effects of CD28 and CTLA-4 are clear cut, distinct functions for B7-1 and B7-2 have yet to be defined. A role in TH_0, TH_1, or TH_2 differentiation has been proposed (Freeman et al. 1995; Kuchroo et al., 1995), but other work (Schweitzer et al., 1997) suggests that B7-1 and B7-2 determine the magnitude of

§To whom correspondence should be addressed (e-mail: david.stuart@strubi.ox.ac.uk and sdavis@molbiol.ox.ac.uk).

costimulatory signals rather than the outcome of TH subset differentiation (reviewed by McAdam et al., 1998). Supporting this view, quantitative rather than qualitative effects on tyrosine phosphorylation follow the stimulation of T cells with artificial antigen-presenting cells expressing B7-1 or B7-2 (Slavik et al., 1999). Moreover, gene disruption studies reveal considerable overlap in the costimulatory functions of B7-1 and B7-2 (Freeman et al., 1993b; Borriello et al., 1997). A third possibility is that, rather than having distinct CD28-dependent costimulatory roles, the key functional differences concern the strength and/or mode of binding of B7-2 and B7-1 to CD28 and CTLA-4.

We have determined the crystal structure of a soluble (s) form of human B7-1 at 3 Å resolution. The structure of the sB7-1 monomer combines features of both the adhesion and antigen receptor subgroups of the IgSF. The arrangement of sB7-1 monomers in the crystal lattice implies that sB7-1 might spontaneously form homodimers, an observation we confirm using analytical ultracentrifugation. These results have important implications regarding the structure and properties of the signaling complexes B7-1 will form in the contact zones between antigen-presenting cells and T cells.

Results

Structure Determination

A histidine-tagged, selenomethionine (SeMet)-labeled form of sB7-1 consisting of residues 1–201 of the mature polypeptide (van der Merwe et al., 1997) was expressed in the Chinese hamster–derived, Lec3.2.8.1 cell line in the presence of 0.5 mM N-butyl deoxynojirimycin and then deglycosylated as described (Butters et al., 1999). Deglycosylated, unlabeled sB7-1 bound CTLA-4 with wild-type affinity (A. V. C. et al., unpublished data). After removal of the histidine tag, crystals of space group $I4_122$ that diffracted to 3 Å resolution at a synchrotron source (BM14 of the European Synchrotron Radiation Facility [ESRF], Grenoble, France) were obtained. The structure was determined using the multiple-wavelength anomalous dispersion (MAD) method.

Overall Structure

The sB7-1 monomer is a slender molecule, with dimensions of $23 \times 30 \times 90$ Å^3, consisting of two anti-parallel β sandwich IgSF domains joined by a short linker region (Figure 1A). Thr-199 forms the last main chain hydrogen bond in the molecule and Ala-200 is well ordered but extends into solution. Between this residue and the probable first residue of the transmembrane domain (Leu-209), the native protein sequence consists of eight, mostly hydrophilic, residues likely to form an extended stalk linking the protein to the cell surface. Overall, the organization and dimensions of sB7-1 resemble those of the extracellular region of CD2 (Figure 1B), although there is a significant change in relative domain orientation (see below).

Immunoglobulin-like Domains

The amino-terminal domain (d1) of B7-1 has V-set topology (Williams and Barclay, 1988), with β strands forming DEB and AGFCC′C″ β sheets. Automated structure comparisons (DALI; Holm and Sander, 1995) rank B7-1d1 as most similar to the membrane distal domains of CD2 (1hnf) and CD4 (1cdy), molecules involved in cell–cell adhesion. Superimpositions of the B7-1, CD2, and antibody ($IgV_L\lambda$) V-set domains are shown in Figure 1C (rms differences between B7-1d1 and CD2d1 and the Ig domain are 1.1 Å and 1.3 Å for 89 and 81 equivalent Cα

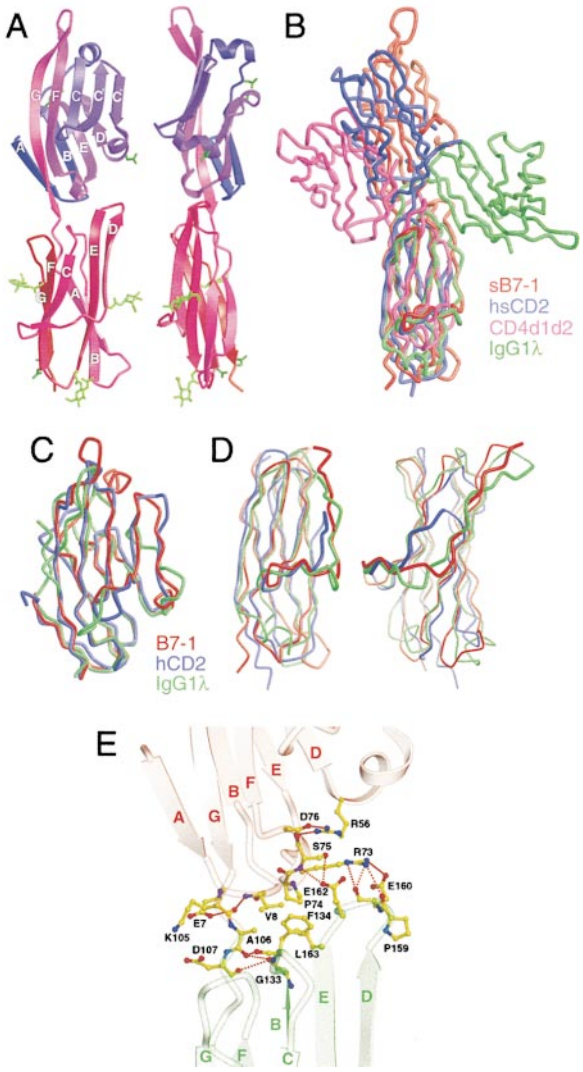

Figure 1. The Structure of the SeMet Form of sB7-1

(A) Two orthogonal views, shown in ribbon format, of the sB7-1 monomer. To indicate the course of the main chain, the color is varied from blue for residue 1 to red for residue 200. Asparagine residues that are part of glycosylation sequons are colored green and modeled with N-acetylglucosamine residues where electron density was sufficiently clear.

(B) Schematic α carbon representations of sB7-1, CD4d1d2 (1cdy), human sCD2 (1hnf), and IgG1 λ light chain (8fab) are shown superimposed on domain 2 of each molecule.

(C) Comparisons of the V-set IgSF domains of B7-1, human CD2 and IgG1 λ light chain.

(D) Two orthogonal views of domain 2 of B7-1 superimposed on the equivalent domains of IgG1 λ light chain and hCD2. The C′ or D strands are highlighted.

(E) The interdomain region of B7-1 with domain 1 and 2 colored red and green, respectively. The network of residues mediating interdomain contacts are shown in ball-and-stick representation.

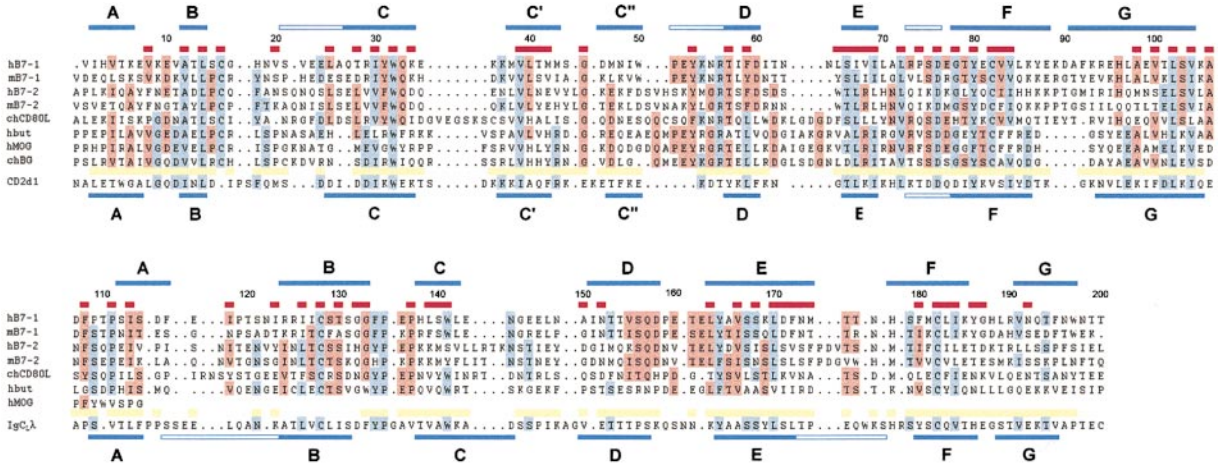

Figure 2. Alignment of B7 Subset and Human CD2 d1 and $IgC_L\lambda$ Sequences Based on the sB7-1, sCD2, and IgG1 λ Light Chain Crystal Structures

The B7 subset, initially defined by Linsley et al. (1994), is extended to include chicken CD80-like protein (chCD80L; TrEMBL accession number O42404). Alignments were done using CLUSTALW (Thompson et al., 1994) and then adjusted by eye. The structural alignments of B7-1 d1 and d2 with CD2 d1 and $IgC_L\lambda$, respectively, are based on the superpositions shown in Figure 1. Residues that are structurally equivalent in the superpositions are highlighted with yellow bars. Open and closed blue bars above the sequences mark α helices and β strands in the sB7-1 structure, respectively. Buried residues (i.e., those exposing less than 25 $Å^2$ of side chain surface area) are highlighted with red bars. Amino acids that exhibit a high degree of conservation in V and C1-set IgSF domains (Barclay et al., 1997) are colored blue, whereas those shaded orange are conserved only within the B7 subset sequences.

atoms, respectively). An important structural similarity shared by B7-1d1 and CD2d1, distinguishing these domains from antigen receptor V-set domains, is the lack of overall twist in the AGFCC′C′′ sheet. This reflects the fact that B7-1d1 has its β bulges located immediately after the CC′ and FG turns at residues Met-38 and Arg-94, (equivalently positioned at residues Lys-43 and Asn-92 in human CD2d1; Bodian et al., 1994) rather than the C′ and G strand β bulges conserved in antigen receptor V-set domains.

In contrast to d1, the membrane proximal domain of B7-1 (d2) exhibits greater similarity to the constant domains of antigen receptors and the membrane proximal domains of MHC antigen-type structures than to the membrane proximal domain of cell–cell adhesion molecules. The d2 β sandwich is formed by DEBA and GFC β sheets typical of C1-set domains (Williams and Barclay, 1988). Thus, the six structures most similar to B7-1d2 selected by DALI all contain C1-set domains, and structural superposition of B7-1d2 with the constant domain of immunoglobulin λ light chain reveals greater similarity than the superposition of B7-1d2 with CD2d2 (rms differences of 1.4 Å and 1.5 Å for 80 and 64 equivalent residues, respectively; Figure 1D). The key structural feature is the organization of the strands at the "edge" of the domain: whereas beyond the C strand, CD2 has two short C′D strands extending the same β sheet, the B7-1 and the Fab C1-set domains have extended DE strands forming the first half of the second β sheet.

Interdomain Region

The interdomain "linkers" of B7-1 and human CD2 are identical in length (seven residues) and share remarkably similar main chain conformations, even though only Pro-111 and Ile-113 are conserved in both sequences (B7-1 sequence numbering). After superimposition of the membrane-proximal domains, the position of the membrane-distal (N-terminal) domain of sB7-1 differs from that of sCD2 by a rotation of 100° about the long axis of the molecule and a reduction of 20° in tilt relative to the same axis. The rotation occurs about Ala-106 of B7-1 (Glu-104 in CD2). The reduced tilt, and the much longer D and E strands of d2, result in the interdomain region of B7-1 burying a larger surface area (670 versus 590 $Å^2$) than is the case for CD2. This region consists of a buried, hydrophobic core formed by Val-8, Pro-74, Ala-106, Phe-134, and Leu-163. In addition, electrostatic contacts and main chain or side chain hydrogen bonds between Ser-75 and Glu-162, and between Arg-73 and both Pro-159 and Glu-160, appear to stabilize the extended, upright stature of the extracellular region of B7-1. The elaborate network of interactions supporting d1 is shown in Figure 1E.

The distinctive features of B7-1 define a new subset of the IgSF, into which sequence analysis groups B7-2, a chicken CD80-like protein (chCD80L), myelin/oligodendrocyte (hMOG) protein, the milk-fat globule membrane protein, butyrophilin (hbut), and the chicken MHC molecule, B-G antigen (chBG; Figure 2; Linsley et al., 1994; O'Regan et al., 1999). Although low, sequence identities indicate that these molecules have similar secondary and tertiary structures. The largest block of conserved residues that are not IgSF consensus residues lie in the D and E β strands and DE loop of domain 2. The conservation of this region, which is involved in the key interdomain electrostatic contacts, along with the conserved hydrophobicity of the interdomain core (residues 8, 106, 134, and 163), suggests that the frameworks of these molecules are likely to be similar.

Ligand Binding

Substantial losses (>90%) in ligand-binding activity occur when the solvent-exposed residues Arg-29, Tyr-31,

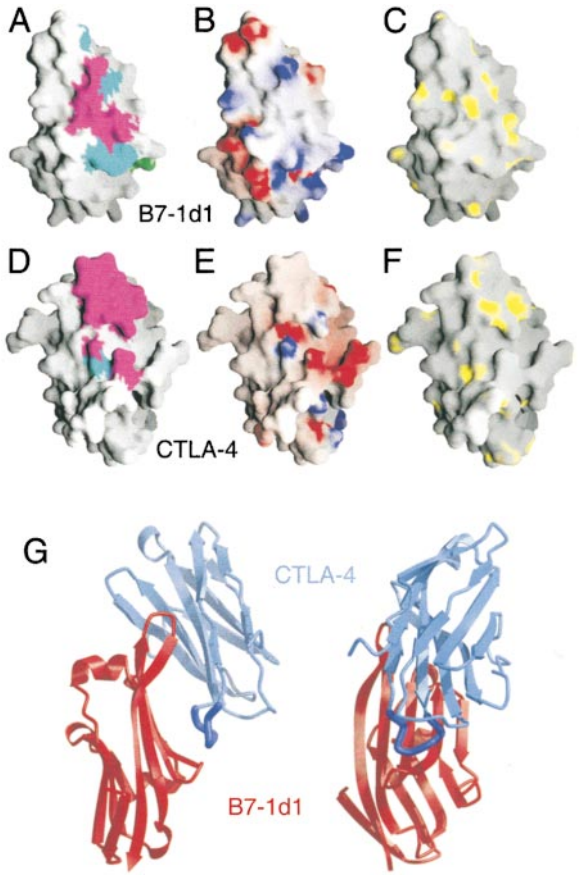

Figure 3. Properties of the Ligand Binding Faces of B7-1d1 and CTLA-4, and a Modeled Complex of these Molecules

In (A) (B7-1d1) and (D) (CTLA-4), the GRASP surfaces of residues whose mutation to alanine disrupts or has no effect on binding (Peach et al., 1995; Metzler et al., 1997) are colored magenta and cyan, respectively. In (B) and (E), the electrostatic potential calculated at neutral pH is shown projected onto the GRASP surfaces of each molecule; blue represents positive potential, white represents neutral, and red represents negative potential contoured at ± 8.5 kT. In (C) and (F), hydrophobicities calculated using GRID (P. Goodford, personal communication) are projected onto the GRASP surfaces of each molecule; yellow highlights regions of greatest hydrophobicity. The line of view in each panel is essentially perpendicular to the AGFCC′C′′ ligand binding face of each molecule. In (G), the MYPPPY sequence of CTLA-4 implicated in B7-1 binding is highlighted as a darker blue loop in these two orthogonal views of the modeled complex.

Gln-33, Met-38, Ile-49, Trp-50, and Lys-86 of B7-1 are substituted with alanine (Figure 3A; Peach et al., 1995). With the exception of Lys-86, these residues form a contiguous, L-shaped cluster identifying the d1 AGFCC′C′′ face as the ligand binding site of B7-1. Lys-86, which is not in the AGFCC′C′′ face, may nevertheless form a salt bridge with Glu-24 in the BC loop that stabilizes the conformation of the FG loop. Not all of the residues surrounding this patch have been mutated, however, and it is likely that the full binding surface is substantially larger than this. Gln-33 is completely conserved in human and mouse B7-1 and B7-2, as are aromatic residues at position 31 and hydrophobic residues at position 38 (Figure 2). The conservation of these residues may explain the cross-reactivities of human and mouse B7-1 and B7-2 with human and mouse CD28 and CTLA-4.

It has been proposed that d2 residues form part of the B7-1 ligand-binding site (Peach et al., 1995). However, the relevant mutations (of DE loop residues Gln-157, Asp-158, and Glu-162) have much weaker effects on ligand binding (<50% inhibition) than mutations of the d1 AGFCC′C′′ face and inspection of the structure suggests that such effects could result from changes in the presentation of d1 via alterations in the network of interactions at the domain interface (Figure 1E). Simple modeling also indicates that CTLA-4 cannot simultaneously bind both sets of residues. Furthermore, direct involvement of d2 would generate B7-1/ligand complexes spanning a much shorter intermembrane distance (~10 nm) than TCR/MHC complexes (~15 nm), creating a steric barrier to the CTLA-4/TCR interactions required for inhibitory signaling by CTLA-4 (Lee et al., 1999). For these reasons, we conclude that the d1 AGFCC′C′′ face represents the principal ligand-binding surface of B7-1.

The AGFCC′C′′ face of B7-1 is compositionally similar to other sites of protein–protein recognition and thus has substantially fewer charged and more hydrophobic residues than the equivalent face of CD2, which is also involved in low-affinity cell surface recognition (29% charged residues versus 45%–70% for CD2 [Bodian et al., 1994; Davis et al., 1998a]). Surface electrostatic potential is depicted in Figure 3B. Two hydrophobic residues essential for ligand binding, Met-38 and Trp-50, form a contiguous hydrophobic patch at the base of the AGFCC′C′′ sheet of d1. In a complementary manner, the conserved MYPPPY sequence motif implicated in the binding of both CTLA-4 and CD28 to B7-1 and B7-2 (Figure 3D; Metzler et al., 1997), forms a hydrophobic patch centered on the FG loop of CTLA-4. The distribution of hydrophobicity on the surfaces of the AGFCC′C′′ face of each molecule is shown in Figures 3C and 3F.

Manual docking of B7-1 d1 and CTLA-4, so that contact between the two hydrophobic patches and electrostatic complementarity are each maximized, and in a way that would permit interactions between adjacent cells, readily generates a feasible model for the complex of these two molecules (Figure 3G). The model is reminiscent of the antiparallel homophilic contacts observed in crystals of Protein 0 (Shapiro et al., 1996) and buries approximately 800 Å^2 of surface area per molecule, an area comparable to that buried in most other protein complexes (Janin and Chothia, 1990). The exaggerated twist of the AGFCC′C′′ β sheet of CTLA-4 could allow extensive contact with the very long FG loop of B7-1, which appears to be a conserved feature of the B7-related sequences (Figure 2).

Molecular Association in the Crystal

A striking and unexpected feature of the sB7-1 crystal lattice is that it is dominated by a molecular contact at the 2-fold axis, which buries 610 Å^2 of surface area for each molecule. The lattice contact generates a compact dimer that, in overall shape and dimensions, is reminiscent of an antibody Fab′ molecule (Figure 4A). However, the dimer differs from a Fab′ insofar as the d1 interaction

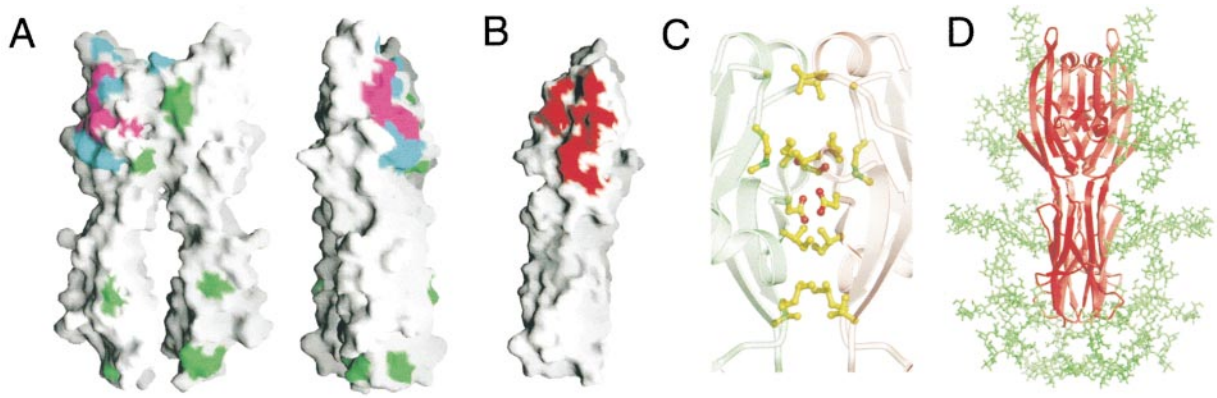

Figure 4. Structure of the sB7-1 Homodimer Observed in the Crystal Lattice

(A) Two orthogonal views of the GRASP surface of the homodimer showing the location of residues whose mutation to alanine disrupts (magenta) or has no effect (cyan) on binding. Putative N-glycosylation sites are colored green.

(B) The GRASP surfaces of amino acids involved in forming the dimer are colored red. The view is identical to the right-hand panel in (A) but with the front copy of sB7-1 removed.

(C) Details of the residues at the dimer interface are shown in ball-and-stick format viewed as in the left-hand panel of (A).

(D) The homodimer is shown with either oligomannose, bi-, or triantennary N-glycans modeled at each of the potential glycosylation sites.

is mediated by a relatively flat surface formed by the B, C′′, D, and E β strands rather than the AGFCC′C′′ face, and there is no contact between d2 of each molecule (although such contacts might be possible in vivo and may only be precluded by this particular lattice). The interaction is mediated by the primarily hydrophobic residues (Val-11, Val-22, Gly-45, Met-47, Ile-58, Asp-60, Ile-61, Thr-62, and Leu-70) decorating the B, C′′, D, and E β strands, leaving the AGFCC′C′′ face free for ligand binding (Figures 4B and 4C). The molecules are inclined by 4° to the 2-fold axis, an arrangement consistent with the C-terminal stalks linking the molecules to the cell surface entering the membrane adjacently. The distribution of the glycosylation sites on the sB7-1 structure indicates that, even if all potential sites were to be fully utilized, the dimer interface would be free of N-linked glycans (Figures 4A and 4D).

Dimerization of sB7-1 in Solution

Analytical ultracentrifugation at a range of concentrations and at three temperatures (Figures 5A and 5B; see Experimental Procedures) indicates that sB7-1 undergoes dimerization in solution with a K_d in the range of 20–50 μM. At higher concentrations, aggregation also occurred (data not shown). These effects are reversible, and sedimentation velocity boundary analysis (Stafford, 1992) of samples in a concentration range where both monomer and dimer were present was unable to differentiate between the species, indicating that monomer and dimer are in rapid exchange with a rate constant of dissociation greater than 10^{-2} s^{-1} (Cann, 1986). The temperature dependence of the K_d is consistent with the largely hydrophobic nature of the contact seen in the crystal lattice.

Discussion

The relationship of the structure of the extracellular region of B7-1 to its function is illuminated by comparison with CD2. A key structural difference between B7-1 and CD2 lies in d2 of each molecule. In B7-1 this domain is topologically similar to C1-set domains, which have

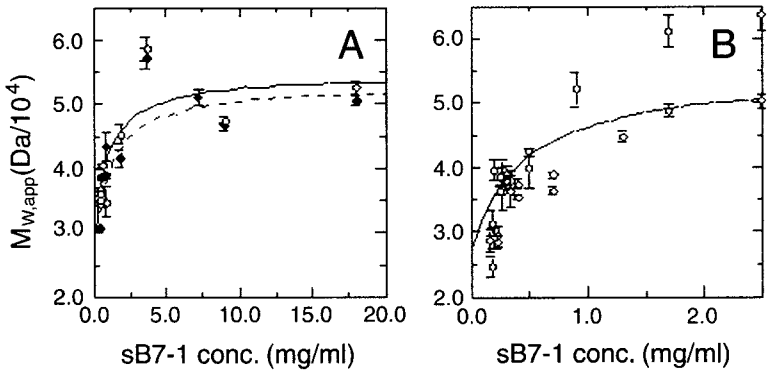

Figure 5. Analytical Ultracentrifugation of sB7-1

Apparent whole-cell weight-average molecular weight ($M_{w,app}$) of sB7-1 as a function of sample loading concentration at 4°C (closed circles) and 20°C (open circles) (A) and at 37°C (open circles) (B). The 4°C (dashed line, [A]), 20°C (solid line, [A]), and 37°C (solid line, [B]) data have been fitted to equation 2 to obtain apparent dissociation constants. The trends in $M_{w,app}$ indicate that sB7-1 is undergoing self-association and is in dynamic equilibrium between a monomeric form ($M_{w,app}$ ~ 27 kDa) and a dimeric form ($M_{w,app}$ ~54 kDa). The parameters given by the fits to the data for sB7-1 are a monomer mass (M_1) of 26609 ± 2206 Da, with a dissociation constant K_d of 44 μM at 4°C; an M_1 of 27384 ± 1942 Da, K_d of 33 μM at 20°C; and an M_1 of 27478 ± 3176 Da, with a dissociation constant K_d of 17 μM at 37°C.

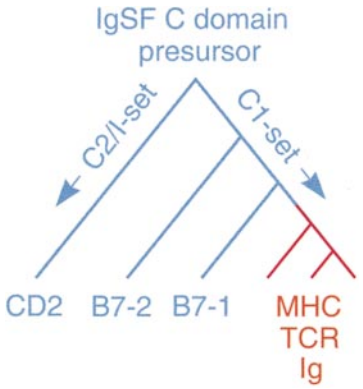

Figure 6. Evolutionary Relationships of the IgSF Constant-like Domains

The parts of the lineage colored blue are proposed to have generated cell adhesion and cell–cell recognition molecules, whereas the red section produced components of the adaptive immune response. CD2 is used to represent the C2/I-set.

previously only been observed in the structures of antigen receptors and MHC antigens; in contrast, CD2d2 belongs to the C2-set. The ALIGN program (Dayhoff et al., 1983) gives significantly higher scores for comparisons of human and mouse B7-1d2 sequences with representative C1-set sequences (Barclay et al., 1997) than for C2-set sequences (5.4 $\pm$ 0.56 versus 2.79 $\pm$ 1.99, respectively). Thus, both topology and sequence place d2 of B7-1 within the C1-set. However, the ALIGN scores for B7-1d2 comparisons with other C1-set sequences are significantly lower than for comparisons within the classic C1-set (8.5 $\pm$ 2.7). This implies that the appearance of B7-1-like molecules may have predated the evolution of distinct antigen receptors and MHC antigens. B7-1 and B7-2, while clearly related, share very limited sequence similarity, and human and mouse B7-2d2 give equally poor matches with both C1- and C2-set sequences (2.3 $\pm$ 0.9 and 2.2 $\pm$ 1.1), suggesting that B7-2 might be even more primitive. Taken with the observation that the adhesion domains of B7-1 and CD2 are remarkably similar, these data suggest a set of evolutionary relationships in which the earliest members of the C1-set are adhesion molecules, and antigen receptors essential for adaptive immune responses (characterized by GFCC′C′′ β sheet mediated V-set heterodimerization [Springer, 1991]) appear late in the evolution of the IgSF (Figure 6). Similarity between domain 2 of B7-1 and the C1-set domain of β2-microglobulin was predicted by Bajorath et al. (1994), and the genetic linkage of B7-related molecules to the MHC has been noted previously (Henry et al., 1997).

Although sB7-1 and sCD2 have similar overall dimensions, the reduced tilt of domain 1 relative to domain 2 positions the ligand binding AGFCC′C′′ face of B7-1 normal to the long axis of the molecule rather than, as in CD2, parallel with it (Jones et al., 1992; Bodian et al., 1994). Such differences may be related to the sequence of expression of these genes. Maximum exposure of the ligand binding face at the "top" of the molecule may be crucial for establishing the initial contact zone between T cells and antigen-presenting cells by CD2 (van der Merwe et al., 1995; Davis and van der Merwe, 1996; Dustin et al., 1998). B7-1 appears after formation of the contact zone, however, when the interacting cell surfaces are already optimally aligned for interactions involving molecules the size of B7-1, the T cell receptor, and their respective ligands. An important consequence of the essentially parallel alignment of d1 and d2 of B7-1 is that it exposes the non-ligand-binding DEB face of d1, allowing the formation of parallel, compact homodimers. The formation of equivalent dimers by CD2 is precluded by the 42° tilt in the position of d1 relative to the long axis of the molecule (Jones et al., 1992; Bodian et al., 1994).

Functionally distinct interactions are suggested by the presence of radically different molecular contacts in the crystal lattices of sB7-1 and sCD2. sCD2 packs head-to-head, an arrangement which was predicted (Jones et al., 1992) and subsequently shown (Wang et al., 1999) to mimic natural receptor-ligand interactions. In contrast, the sB7-1 crystal lattice is dominated by a side–side molecular contact that generates a potentially bivalent homodimer. Model studies indicate that cell surface proteins with solution affinities in the range of 15–75 μM interact spontaneously at membrane interfaces (Dustin et al. 1996; 1997). The K_d of 20–50 μM for dimerization and rapid monomer–dimer exchange we have observed

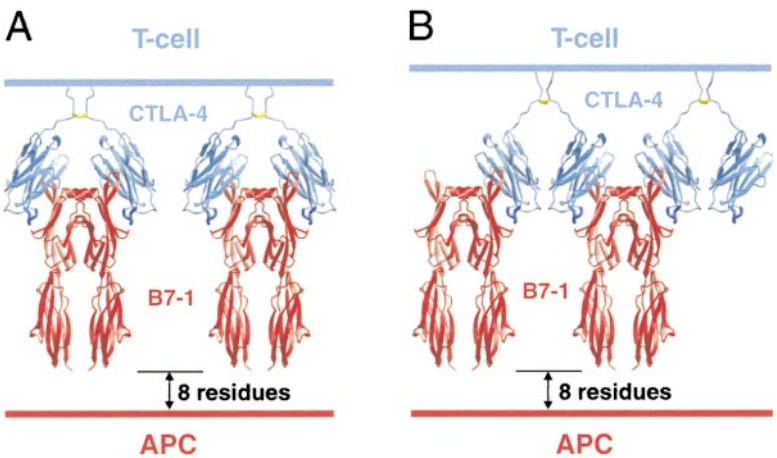

Figure 7. Potential Molecular Complexes Formed by the B7-1 and CTLA-4 Homodimers at the Cell Surface

The B7-1 homodimer shown is identical to that observed in the crystal lattice. The CTLA-4 homodimer is based on the solution structure of the monomer (Metzler et al., 1997), with the sequence connecting β strand G to the intermolecular disulphide at Cys-123 modeled in extended conformation. The ligand-binding domains of B7-1 and CTLA-4 are docked as described in the text, allowing the formation of two potential types of complexes: paired homodimers (A) and complexes in which separate sB7-1 homodimers are bridged by adjacent CTLA-4 dimers (B).

Table 1. Data Collection and Refinement Statistics

Data Processing				
Wavelength (Å)	0.8855	0.9793	0.9796	all
Observation	34,375	34,531	36,114	105,456
Unique*	9,341	9,349	9,436	5,409
Redundancy	3.7	3.7	3.8	19.5
$<I/\sigma(I)>$	12 (3)	10 (2)	11 (2)	24 (5)
R_{merge} (%)	9.2 (42)	9.3 (43)	9.2 (42)	11.4 (48)
Resolution (Å)		20–3.0 (3.1–3.0)		
Completeness (%)	98 (93)	99 (96)	99 (93)	100 (99)

Refinement	
Data range (Å)	20–3.0 (3.1–3.0)
Reflections (F>0)	5,204 (283)
Completeness (%)	96.5 (88.9)
Reflections in R_{free} set	289 (21)
Nonhydrogen atoms (protein/sugar)	1,604/42
Rms Δ bond lengths (Å)	0.008
Rms Δ bond angles (°)	1.4
Rms Δ B factors for bonded atoms (Å^2) (main/side)	1.3/1.9
Mean B factors (Å^2) (main/side/sugar)	41.4/42.8/49.0
Mean main chain B factors (Å^2) (domain 1/domain 2)	45.2/37.2
R_{free} (%)	28.2 (35.4)
R_{cryst} (%)	23.7 (34.1)

* For data sets collected at individual wavelengths, Bijvoet pairs were not merged. However, the Bijvoet pairs were merged in the data set generated by merging the data collected at all wavelengths.
Values in parentheses correspond to the highest resolution shell (3.1–3.0 Å).
$R_{merge} = \Sigma|I - <I>|/\Sigma<I>$
$R_{cryst} = \Sigma||F_{obs}| - |F_{calc}||/\Sigma|F_{obs}|$
R_{free} = as for R_{cryst} but calculated for a test set comprising reflections not used in the refinement.
Root mean squared deviations (rms Δ) in bond length and angles are given from ideal values.

suggests that B7-1 may exist at the cell surface in a dynamic equilibrium dominated by a homodimer similar to that observed in the crystal. Since CTLA-4 exists as a disulfide-bonded homodimer, the existence of B7-1 dimers would allow two types of multivalent associations to form at the cell–cell interface, one involving paired homodimers (Figure 7A), the alternative involving a dimer of B7-1 bridging adjacent CTLA-4 dimers (Figure 7B). Simple modeling studies suggest that the second type of interaction might be sterically favored.

CTLA-4 is not expressed on resting T cells, and the level of CTLA-4 expression at the cell surface is kept very low, even on activated cells (Linsley et al., 1992a). CTLA-4 is also stored in intracellular vesicles (Leung et al., 1995) whose release is directed at the contact zone between activated T cells and antigen-presenting cells (Linsley et al., 1996). This suggests that its release into and sequestration within the central supramolecular activation cluster (cSMAC) of the immunological synapse (Monks et al., 1998; Grakoui et al., 1999) is key to the inhibitory function of CTLA-4. The solution affinity of B7-1 for CTLA-4 (~0.2–0.4 μM) is among the highest described for interacting cell surface molecules (reviewed in Davis et al., 1998b), at least 10-fold higher than the affinity of B7-1/CD28 interactions (~4 μM; van der Merwe et al., 1997) and 40- to 100-fold higher than that of B7-2/CD28 interactions (~15 μM; A. V. C. et al., unpublished data). The avidity model proposed in Figure 7B would provide a mechanism for further stabilizing the interaction of B7-1 with CTLA-4 within the cSMAC. While it is clear that B7-1/CD28 interactions may generate competing costimulatory signals, the foregoing structural considerations, along with the timing of B7-1 and CTLA-4 expression, suggest that a key function of B7-1 is to generate particularly stable signaling complexes with CTLA-4 late in immune responses, increasing the likelihood of inhibitory signaling by CTLA-4 and facilitating the termination of T cell activation.

Experimental Procedures

Protein Expression and Crystallization

The expression of a construct encoding a histidine-tagged form of sB7-1, consisting of residues 1–201 of the native protein and bearing a deleted C-terminal glycosylation site (Asn-198), in Lec3.2.8.1 cells in the presence of 0.5 mM N-butyl deoxynojirimycin is described by Butters et al. (1999). SeMet labeling was done according to the method of May et al. (1997). After removal of the histidine tag with carboxypeptidase A (van der Merwe et al., 1997), data collection–quality wild-type and SeMet sB7-1 crystals grew readily in sitting drops containing 2 μl of protein (at an optical density of 20–30 in 10 mM HEPES, 140 mM NaCl, 0.05% NaN_3 [pH 7.4]) and 2 μl of reservoir solution (typically a 10%–90% v/v dilution of a stock solution containing 28% PEG 400, 0.1M Na HEPES (pH 7.5), 0.2M $CaCl_2$).

Structure Determination

The crystals belong to space group $I4_122$ (cell dimensions a = b = 57.3 Å, c = 298.9 Å, consistent with a single molecule per asymmetric unit). For data collection at 100 K, crystals were briefly transferred to mother liquor containing 10% v/v glycerol. Molecular replacement and multiple isomorphous replacement phasing attempts failed (high levels of nonisomorphism were apparent between native and heavy atom data sets). Diffraction data for MAD-based phase determination were collected from one cryo-cooled SeMet sB7-1 crystal at station BM14 of the ESRF. The Se absorption edge was located by a fluorescence scan, and consecutive data sets were collected at three wavelengths (λ = 0.8855 Å, 0.97930 Å, and 0.97955 Å, the latter wavelengths being at the white line and inflection point) using

the 180 mm scan mode of a 345 mm diameter MAR-Research (Hamburg, Germany) image plate detector. The diffraction data were processed and scaled with the HKL program suite (Otwinowski and Minor, 1997; statistics reported in Table 1). The expected six Se atom positions were determined, refined, and phases calculated to 3.0 Å resolution, using the program SOLVE (Terwilliger and Berendzen, 1997). An initial electron density map based on these phases was improved with programs DM and SOLOMON (CCP4, 1994) to yield a high quality electron density map. The structure was built using program O (Jones et al., 1991). The entire course of the main chain was apparent; however, only half the true side chains were built, with the remainder initially modeled as alanines.

Refinement with CNS (Brunger et al., 1998) used a set of F_{obs} constructed by merging the diffraction data (including Bjivoet pairs) from all three MAD wavelengths. After some refinement and manual rebuilding, the entire sB7-1 sequence was fitted and clear electron density allowed the unambiguous positioning of three N-linked N-acetylglucosamine residues. Further refinement of the atomic positions and tightly restrained individual isotropic B-factors resulted in a final crystallographic R_{factor} and R_{free} of 23.7% and 28.2%, respectively. In the final model, 80.4% of residues fall in the most favored regions of the Ramachandran plot and no nonglycine residues fall in disallowed regions (Laskowski et al., 1993). Refinement and model statistics are reported in Table 1.

Structural superpositions used program SHP (Stuart et al., 1979). Figures 1–3, 6, 7, and 9 were produced using programs BOBSCRIPT (Esnouf, 1997) and Raster3D (Merritt and Murphy, 1994). Electrostatic analysis and surface display for Figures 5 and 7 used the program GRASP (Nicholls et al., 1991).

Analytical Ultracentrifugation Methods

Analytical ultracentrifugation used a Beckman Instruments Optima XL-A equipped with scanning absorbance optics utilizing wavelengths of 225 nm, 230 nm, 254 nm, 280 nm, 300 nm, 310 nm, and 320 nm, depending on the protein concentrations present (Tuma et al., 1996). Thermodynamic equilibrium was taken to have been reached when distribution scans acquired 3 hr apart were coincident. The experiments were performed at a rotor speed of 10,000 rpm, and the sample was pelleted from solution at 40,000 rpm following the attainment of equilibrium to allow the baseline absorbance to be measured. The data were fitted with the equation

$$A(r) = A(r_F)\exp\left[\frac{(1 - \bar{\nu}\rho)\omega^2}{2RT}(r^2 - r_F^2)\right] + E \quad (1)$$

where $A(r)$ is the absorbance at radius r (in cm), $A(r_F)$ is the absorbance at reference radius r_F, $\bar{\nu}$ is the partial specific volume (in ml/g), ρ is the solvent density (in g/ml), ω is the angular velocity of the centrifuge rotor (in rad/s), R is the gas constant, T the absolute temperature, and E the baseline offset. By comparing the apparent mass of the glycosylated sB7-1 molecules determined using SDS-PAGE with the known mass of the polypeptide alone, the percent by weight sugar was estimated. The weighted average $\bar{\nu}$ was calculated as 0.687 ml/g using known values for the partial volumes of amino acids and sugars (Perkins, 1986). The whole-cell weight-average apparent molecular weights obtained through fitting Equation 1 to the equilibrium distributions were plotted against the concentration at the midpoint of the distribution (Laue, 1992) to obtain diagnostics of the solution behavior of the samples. These curves were fitted with the equation

$$M_{w,app} = \frac{(n - 1)M_1 c}{K_d + c} + M_1 \quad (2)$$

where $M_{w,app}$ is the apparent whole-cell weight-average molecular weight (in Da) obtained from fitting equation 1, n is the association state of the complex formed by the protein, M_1 is the monomer mass of the protein, c is the protein concentration, and K_d is the dissociation constant of the protein complex (in units of c).

Acknowledgments

The authors thank P. Sorensen, V. Avery, P. A. van der Merwe, and W. F. Stafford for advice and comments on the manuscript and B. J. Classon for assistance with the sequence comparisons. This work was supported by the Arthritis Research Campaign, the Biotechnology and Biological Sciences Research Council, the Engineering and Physical Sciences Research Council, the Medical Research Council, the Royal Society and the Wellcome Trust. S. I. and D. I. S. are members of the Tsukuba Advanced Research Alliance project of Tsukuba University, Tsukuba, Japan. The analytical ultracentrifugation experiments were performed in the AUC facility established by the BBSRC and the Wellcome Trust in the Glycobiology Institute of the University of Oxford. The facility is managed by Dr. Russell Wallis.

Received November 2, 1999; revised December 16, 1999.

References

Aruffo, A., and Seed, B. (1987). Molecular cloning of a CD28 cDNA by a high-efficiency COS cell expression system. Proc. Natl. Acad. Sci. USA *84*, 8573–8577.

Azuma, M., Ito, D., Yagita, H., Okumura, K., Phillips, J.H., Lanier, L.L., and Somoza, C. (1993). B70 antigen is a second ligand for CTLA-4 and CD28. Nature *366*, 76–79.

Bajorath, J., Peach, R.J., and Linsley, P.S. (1994). Immunoglobulin fold characteristics of B7-1 (CD80) and B7-2 (CD86). Protein Sci. *3*, 2148–2150.

Barclay, A.N., Brown, M.H., Law, S.K.A., McKnight, A.J., Tomlinson, M.G., and van der Merwe, P.A. (1997). The Leukocyte Antigen Factsbook (London: Academic Press).

Bodian, D.L., Jones, E.Y., Harlos, K., Stuart, D.I., and Davis, S.J. (1994). Crystal structure of the extracellular region of the human cell adhesion molecule CD2 at 2.5 Å resolution. Structure *15*, 755–766.

Borriello, F., Sethna, M.P., Boyd, S.D., Schweitzer, A.N., Tivol, E.A., Jacoby, D., Strom, T.B., Simpson, E.M., Freeman, G.J., and Sharpe, A.H. (1997). B7-1 and B7-2 have overlapping, critical roles in immunoglobulin class switching and germinal center formation. Immunity *6*, 303–313.

Brunet, J.F., Denizot, F., Luciani, M.F., Roux-Dosseto, M., Suzan, M., Mattei, M.G., and Golstein, P. (1987). A new member of the immunoglobulin superfamily—CTLA-4. Nature *328*, 267–270.

Brunger, A.T., Adams, P.D., Clore, G.M., DeLano, W.L., Gros, P., Grosse-Kunstleve, R.W., Jiang, J.S., Kuszewski, J., Nilges, M., Pannu, N.S., et al. (1998). Crystallography and NMR system: a new software suite for macromolecular structure determination. Acta Crystallogr. D Biol. Crystallogr. *54*, 905–921.

Butters, T.D., Sparks, L.M., Harlos, K., Ikemizu, S., Stuart, D.I., Jones, E.Y., and Davis, S.J. (1999). Additive effects of *N*-butyldeoxynojirimycin and the Lec3.2.8.1 mutant phenotype on N-glycan processing in chinese hamster ovary cells: application to glycoprotein crystallisation. Proteins *8*, 1707–1712.

Cann, J.R. (1986). Effects of microheterogeneity on sedimentation patterns of interacting proteins and the sedimentation behavior of systems involving two ligands. Methods Enzymol. *130*, 19–35.

CCP4 (1994). Collaborative Computational Project, Number 4. The CCP4 suite: programs for protein crystallography. Acta Cryst. D *50*, 760–763.

Chen, L., Ashe, S., Brady, W.A., Hellstrom, I., Hellstrom, K.E., Ledbetter, J.A., McGowan, P., and Linsley P.S. (1992). Costimulation of antitumor immunity by the B7 counterreceptor for the T lymphocyte molecules CD28 and CTLA-4. Cell *71*, 1093–1102.

Davis, S.J., and van der Merwe, P.A. (1996). The structure and ligand interactions of CD2: implications for T-cell function. Immunol. Today *17*, 177–187.

Davis, S.J., Davies, E.A., Tucknott, M.G., Jones, E.Y., and van der Merwe, P.A. (1998a). The role of charged residues mediating low affinity protein-protein recognition at the cell surface by CD2. Proc. Natl. Acad. Sci. USA *95*, 5490–5494.

Davis, S.J., Ikemizu, S., Wild, M.K., and van der Merwe, P.A. (1998b). CD2 and the nature of protein interactions mediating cell-cell recognition. Immunol. Rev. *163*, 217–236.

Dayhoff, M.O., Barker, W.C., and Hunt, L.T. (1983). Establishing homologies in protein sequences. Methods Enzymol. *91*, 524–545.

Dustin, M.L., Ferguson, L.M., Chan, P.Y., Springer, T.A, and Golan, D.E. (1996). Visualization of CD2 interaction with LFA-3 and determination of the two-dimensional dissociation constant for adhesion receptors in a contact area. J. Cell. Biol. *132*, 465–474.

Dustin, M.L., Golan, D.E., Zhu, D.M., Miller, J.M., Meier, W., Davies, E.A., and van der Merwe, P.A. (1997). Low affinity interaction of human or rat T cell adhesion molecule CD2 with its ligand aligns adhering membranes to achieve high physiological affinity. J. Biol. Chem. *272*, 30889–30898.

Dustin, M.L., Olszowy, M.W., Holdorf, A.D., Li, J., Bromley, S., Desai, N., Widder, P., Rosenberger, F., van der Merwe, P.A., Allen, P.M., and Shaw, A.S. (1998). A novel adaptor protein orchestrates receptor patterning and cytoskeletal polarity in T-cell contacts. Cell *94*, 667–677.

Esnouf, R.M. (1997). An extensively modified version of MolScript that includes greatly enhanced coloring capabilities. J. Mol. Graph. Model. *15*, 132–134, 112–113.

Finck, B.K., Linsley, P.S., and Wofsy, D. (1994). Treatment of murine lupus with CTLA4Ig. Science *265*, 1225–1227.

Freeman, G.J., Freedman, A.S., Segil, J.M., Lee, G., Whitman, J.F., and Nadler, L.M. (1989). B7, a new member of the Ig superfamily with unique expression on activated and neoplastic B cells. J. Immunol. *143*, 2714–2722.

Freeman, G.J., Gribben, J.G., Boussiotis, V.A., Ng, J.W., Restivo, V.A., Jr., Lombard, L.A., Gray, G.S., and Nadler, L.M. (1993a). Cloning of B7-2: a CTLA-4 counter-receptor that costimulates human T cell proliferation. Science *262*, 909–911.

Freeman, G.J., Borriello, F., Hodes, R.J., Reiser, H., Hathcock, K.S., Laszlo, G., McKnight, A.J., Kim, J., Du, L., Lombard, D.B., et al. (1993b). Uncovering of functional alternative CTLA-4 counter-receptor in B7-deficient mice. Science *262*, 907–909.

Freeman, G.J., Boussiotis, V.A., Anumanthan, A., Bernstein, G.M., Ke, X.Y., Rennert, P.D., Gray, G.S., Gribben, J.G., and Nadler, L.M. (1995). B7-1 and B7-2 do not deliver identical costimulatory signals, since B7-2 but not B7-1 preferentially costimulates the initial production of IL-4. Immunity *2*, 523–532.

Grakoui, A., Bromley, S.K., Sumen, C., Davis, M.M., Shaw, A.S., Allen, P.M., and Dustin, M.L. (1999). The immunological synapse: a molecular machine controlling T cell activation. Science *285*, 221–227.

Greenfield, E.A., Nguyen, K.A., and Kuchroo, V.K. (1998). CD28/B7 costimulation: a review. Crit. Rev. Immunol. *18*, 389–418.

Guinan, E.C., Boussiotis, V.A., Neuberg, D., Brennan, L.L., Hirano, N., Nadler, L.M., and Gribben, J.G. (1999). Transplantation of anergic histoincompatible bone marrow allografts. N. Engl. J. Med. *340*, 1704–1714.

Harding, F.A., McArthur, J.G., Gross, J.A., Raulet, D.H., and Allison, J.P. (1992). CD28-mediated signaling co-stimulates murine T cells and prevents induction of anergy in T-cell clones. Nature *356*, 607–609.

Henry, J., Ribouchon, M., Depetris, D., Mattei, M., Offer, C., Tazi-Ahnini, R., and Pontarotti, P. (1997). Cloning, structural analysis, and mapping of the B30 and B7 multigenic families to the major histocompatibility complex (MHC) and other chromosomal regions. Immunogenetics *46*, 383–395.

Holm, L., and Sander, C. (1995). Dali: a network tool for protein structure comparison. Trends Biochem. Sci. *20*, 478–480.

Hutloff, A., Dittrich, A.M., Beier, K.C., Eljaschewitsch, B., Kraft, R., Anagnostopoulos, I., and Kroczek, R.A. (1999). ICOS is an inducible T-cell co-stimulator structurally and functionally related to CD28. Nature *397*, 263–266.

Janin, J., and Chothia, C. (1990). The structure of protein-protein recognition sites. J. Biol. Chem. *265*, 16027–16030.

Jones, E.Y., Davis, S.J., Williams, A.F., Harlos, K., and Stuart, D.I. (1992). Crystal structure at 2.8 Å resolution of a soluble form of the cell adhesion molecule CD2. Nature *360*, 232–239.

Jones, T.A., Zou, J.Y., Cowan, S.W., and Kjeldgaard, M. (1991). Improved methods for finding protein models in electron density maps and the location of errors in these models. Acta Crystallogr. A *47*, 110–119.

Kuchroo, V.K., Das, M.P., Brown, J.A., Ranger, A.M., Zamvil, S.S., Sobel, R.A., Weiner, H.L., Nabavi, N., and Glimcher, L.H. (1995). B7-1 and B7-2 costimulatory molecules activate differentially the Th1/Th2 developmental pathways: application to autoimmune disease therapy. Cell *80*, 707–718.

Larsen, C.P., Elwood, E.T., Alexander, D.Z., Ritchie, S.C., Hendrix, R., Tucker-Burden, C., Cho, H.R., Aruffo, A., Hollenbaugh, D., Linsley, P.S., et al. (1996). Long-term acceptance of skin and cardiac allografts after blocking CD40 and CD28 pathways. Nature *381*, 434–438.

Laskowski, R.A., MacArthur, M.W., Moss, D.S., and Thornton, J.M. (1993). PROCHECK: a program to check the stereochemical quality of protein structures. J. Appl. Cryst. *26*, 283–291.

Laue, T.M. (1992). Technical Information DS-835 (Palo Alto, CA: Spinco Business Unit).

Leach, D.R., Krummel, M.F., and Allison, J.P. (1996). Enhancement of antitumor immunity by CTLA-4 blockade. Science *271*, 1734–1736.

Lee, K.M., Chuang, E., Griffin, M., Khattri, R., Hong, D.K., Zhang, W., Straus, D., Samelson, L.E., Thompson, C.B., and Bluestone, J.A. (1999). Molecular basis of T cell inactivation by CTLA-4. Science *282*, 2263–2266.

Lenschow, D.J., Walunas, T.L., and Bluestone, J.A. (1996). CD28/B7 system of T cell costimulation. Annu. Rev. Immunol. *14*, 233–258.

Leung, H.T., Bradshaw, J., Cleaveland, J.S., and Linsley, P.S. (1995). Cytotoxic T lymphocyte-associated molecule-4, a high-avidity receptor for CD80 and CD86, contains an intracellular localization motif in its cytoplasmic tail. J. Biol. Chem. *270*, 25107–25114.

Linsley, P.S., Greene, J.L., Tan, P., Bradshaw, J., Ledbetter, J.A., Anasetti, C., and Damle, N.K. (1992a). Coexpression and functional cooperation of CTLA-4 and CD28 on activated T lymphocytes. J. Exp. Med. *176*, 1595–1604.

Linsley, P.S., Wallace, P.M., Johnson, J., Gibson, M.G., Greene, J.L., Ledbetter, J.A., Singh, C., and Tepper, M.A. (1992b). Immunosuppression in vivo by a soluble form of the CTLA-4 T cell activation molecule. Science *257*, 792–795.

Linsley, P.S., Peach, R., Gladstone, P., and Bajorath, J. (1994). Extending the B7 (CD80) gene family. Protein Sci. *3*, 1341–1343.

Linsley, P.S., Bradshaw, J., Greene, J., Peach, R., Bennett, K.L., and Mittler, R.S. (1996). Intracellular trafficking of CTLA-4 and focal localization towards sites of TCR engagement. Immunity *4*, 535–543.

Mandelbrot, D.A., McAdam, A.J., and Sharpe, A.H. (1999). B7-1 or B7-2 is required to produce the lymphoproliferative phenotype in mice lacking cytotoxic T lymphocyte-associated antigen 4 (CTLA-4). J. Exp. Med. *189*, 435–440.

Marengere, L.E., Waterhouse, P., Duncan, G.S., Mittrucker, H.W., Feng, G.S., and Mak, T.W. (1996). Regulation of T cell receptor signaling by tyrosine phosphatase SYP association with CTLA-4. Science *272*, 1170–1173.

Martin, P.J., Ledbetter, J.A., Morishita, Y., June, C.H., Beatty, P.G., and Hansen, J.A. (1986). A 44 kilodalton cell surface homodimer regulates interleukin 2 production by activated human T lymphocytes. J. Immunol. *136*, 3282–3287.

May, A.P., Robinson, R.C., Aplin, R.T., Bradfield, P., Crocker, P.R., and Jones, E.Y. (1997). Expression, crystallization, and preliminary X-ray analysis of a sialicacid-binding fragment of sialoadhesin in the presence and absence of ligand. Protein Sci. *6*, 717–721.

McAdam, A.J., Schweitzer, A.N., and Sharpe, A.H. (1998). The role of B7 co-stimulation in activation and differentiation of CD4+ and CD8+ T cells. Immunol. Rev. *165*, 231–247.

Merritt, E.A., and Murphy, M.E.P. (1994). Raster3D version 2.0: a program for photorealistic molecular graphics. Acta Cryst. D *50*, 869–873.

Metzler, W.J., Bajorath, J., Fenderson, W., Shaw, S.Y., Constantine, K.L., Naemura, J., Leytze, G., Peach, R.J., Lavoie, T.B., Mueller, L., and Linsley, P.S. (1997). Solution structure of human CTLA-4 and delineation of a CD80/CD86 binding site conserved in CD28. Nat. Struct. Biol. *4*, 527–531.

Monks, C.R., Freiberg, B.A., Kupfer, H., Sciaky, N., and Kupfer, A.

(1998). Three-dimensional segregation of supramolecular activation clusters in T cells. Nature *395*, 82–86.

Nicholls, A., Sharp, K.A., and Honig, B. (1991). Protein folding and association: insights from the interfacial and thermodynamic properties of hydrocarbons. Proteins *11*, 281–296.

Olsson, C., Riebeck, K., Dohlsten, M., and Michaelsson, E. (1999). CTLA-4 ligation suppresses CD28-induced NF-kappaB and AP-1 activity in mouse T cell blasts. J. Biol. Chem. *274*, 14400–14405.

O'Regan, M.N., Parsons, K.R., Tregaskes, C.A., and Young, J.R. (1999). A chicken homologue of the co-stimulating molecule CD80 which binds to mammalian CTLA-4. Immunogenetics *1*, 68–71.

Otwinowski, Z., and Minor, W. (1997). Processing of X-ray diffraction data collected in oscillation mode. Methods Enzymol. *276*, 307–326.

Peach, R.J., Bajorath, J., Naemura, J., Leytze, G., Greene, J., Aruffo, A., and Linsley, P.S. (1995). Both extracellular immunoglobin-like domains of CD80 contain residues critical for binding T cell surface receptors CTLA-4 and CD28. J. Biol. Chem. *8*, 21181–21187.

Perkins, S.J. (1986). Protein volumes and hydration effects. The calculations of partial specific volumes, neutron scattering matchpoints and 280-nm absorption coefficients for proteins and glycoproteins from amino acid sequences. Eur. J. Biochem. *157*, 169–180.

Schweitzer, A.N., Borriello, F., Wong, R.C., Abbas, A.K., and Sharpe, A.H. (1997). Role of costimulators in T cell differentiation: studies using antigen-presenting cells lacking expression of CD80 or CD86. J. Immunol. *158*, 2713–2722.

Shapiro, L., Doyle, J.P., Hensley, P., Colman, D.R., and Hendrickson, W.A. (1996). Crystal structure of the extracellular domain from P0, the major structural protein of peripheral nerve myelin. Neuron *17*, 435–449.

Slavik, J.M., Hutchcroft, J.E., and Bierer, B.E. (1999). CD80 and CD86 are not equivalent in their ability to induce the tyrosine phosphorylation of CD28. J. Biol. Chem. *274*, 3116–3124.

Springer, T.A. (1991). Cell adhesion. A birth certificate for CD2. Nature *353*, 704–705.

Stafford, W.F., III (1992). Boundary analysis in sedimentation transport experiments: a procedure for obtaining sedimentation coefficient distributions using the time derivative of the concentration profile. Anal. Biochem. *203*, 295–301.

Stuart, D.I., Levine, M., Muirhead, H., and Stammers, D.K. (1979). Crystal structure of cat muscle pyruvate kinase at a resolution of 2.6 Å. J. Mol. Biol. *134*, 109–142.

Terwilliger, T.C., and Berendzen, J. (1997). Bayesian MAD phasing. Acta Cryst. D *53*, 571–579.

Thompson, J.D., Higgins, D.G., and Gibson, T.J. (1994). CLUSTAL W: improving the sensitivity of progressive multiple sequence alignment through sequence weighting, position-specific gap penalties and weight matrix choice. Nucleic Acids Res. *22*, 4673–4680.

Townsend, S.E., and Allison, J.P. (1993). Tumor rejection after direct costimulation of CD8+ T cells by B7-transfected melanoma cells. Science *259*, 368–370.

Tuma, R., Bamford, J.H., Bamford, D.H., Russell, M.P., and Thomas, G.J., Jr. (1996). Structure, interactions and dynamics of PRD1 virus I. Coupling of subunit folding and capsid assembly. J. Mol. Biol. *257*, 87–101.

van der Merwe, P.A., McNamee, P.N., Davies, E.A., Barclay, A.N., and Davis, S.J. (1995). Topology of the CD2-CD48 cell-adhesion molecule complex: implications for antigen recognition by T cells. Curr. Biol. *5*, 74–84.

van der Merwe, P.A., Bodian, D.L., Daenke, S., Linsley, P., and Davis, S.J. (1997). CD80 (B7-1) binds both CD28 and CTLA-4 with a low affinity and very fast kinetics. J. Exp. Med. *185*, 393–403.

Viola, A., Schroeder, S., Sakakibara, Y., and Lanzavecchia, A. (1999). T lymphocyte costimulation mediated by reorganization of membrane microdomains. Science *283*, 680–682.

Walunas, T.L., Lenschow, D.J., Bakker, C.Y., Linsley, P.S., Freeman, G.J., Green, J.M., Thompson, C.B., and Bluestone, J.A. (1994). CTLA-4 can function as a negative regulator of T cell activation. Immunity *1*, 405–413.

Wang, J.H., Smolyar, A., Tan, K., Liu, J.H., Kim, M., Sun, Z.Y., Wagner, G., and Reinherz, E.L. (1999). Structure of a heterophilic adhesion complex between the human CD2 and CD58(LFA-3) counterreceptors. Cell *97*, 791–803.

Waterhouse, P., Penninger, J.M., Timms, E., Wakeham, A., Shahinian, A., Lee, K.P., Thompson, C.B., Griesser, H., and Mak, T.W. (1995). Lymphoproliferative disorders with early lethality in mice deficient in Ctla-4. Science *270*, 985–988.

Weiss, A., Manger, B., and Imboden, J. (1986). Synergy between the T3/antigen receptor complex and Tp44 in the activation of human T cells. J. Immunol. *137*, 819–825.

Williams, A.F., and Barclay, A.N. (1988). The immunoglobulin superfamily—domains for cell surface recognition. Annu. Rev. Immunol. *6*, 381–405.

Wülfing, C., and Davis, M.M. (1999). A receptor/cytoskeletal movement triggered by costimulation during T cell activation. Science *282*, 2266–2269.

Protein Data Bank Coordinates

The coordinates of the sB7-1 monomer structure have been deposited in the Protein Data Bank (PDB ID 1DR9).